

Electro-Mechanical Control of Hexapod Robot Locomotion

Ezequiel del Rio, Valeri A. Makarov, Manuel G. Velarde, Manuel G. Bedia, and Werner Ebeling,

Abstract—A nonlinear closed lattice or ring is proposed as a central pattern generator (CPG) for controlling hexapodal robots. We show that the ring composed of six anharmonically interacting units coupled to the limb actuators permits to reproduce typical hexapod gaits. We provide an electronic circuit implementation of the CPG providing the corresponding gaits. Then we propose a method to incorporate the actuator (motor) and leg dynamics in the units of the CPG. With this electro-mechanical device we close the loop CPG – environment – CPG, thus obtaining a decentralized approach for the leg control that does not require higher level CPG intervention during locomotion in a non-smooth hence non flat landscape. The gaits generated by our CPG are not rigid, but adapt to obstacles faced by the robot.

Index Terms—Legged locomotion, manipulator dynamics, nonlinear circuits

I. INTRODUCTION

Animal locomotion seems to be driven by a central pattern generator (CPG), which is an intra-spinal network of neurons capable of generating a rhythmic output required for the limb control [1]. The study of CPGs is crucial for understanding both the global animal behavior and particular functions of such neural networks. Besides it is also important for designing neuro-inspired robots capable to move in an efficient manner in almost arbitrary landscapes or environments.

Research on the leg coordination and movement has been shifted from descriptive studies [2] to investigations of the neurophysiological mechanisms and control of walking [3]. Leg movement seems to be an intrinsic part of the step pattern generator rather than merely the reflection of activity in a high level CPG [4]. The architecture of CPGs is seldom observable in vivo. However, important aspects of their structure can be inferred from observation of gait features such as the phase

E. del Rio is with the Department of Applied Physics, E.T.S.I. Aeronauticos, Universidad Politecnica de Madrid, Plaza Cardenal Cisneros, 3, E-28040 Madrid, Spain (e-mail: edelrio@aero.upm.es).

V. A. Makarov is with Escuela de Optica, Universidad Complutense de Madrid, Avda. Arcos de Jalon s/n, E-28037 Madrid, Spain (e-mail: vmakarov@opt.ucm.es).

M. G. Velarde is with Instituto Pluridisciplinar, Universidad Complutense de Madrid, Paseo Juan XXIII, 1, E-28040 Madrid, Spain (e-mail: mvelarde@pluri.ucm.es).

M. G. Bedia is with Escuela Politecnica Superior, Universidad Carlos III, Avda. de la Universidad, 30, E-28911 Leganes, Madrid, Spain.

W. Ebeling is with Institut für Physik, Humboldt-Universität Berlin, Newtonstr., 15, 12489 Berlin, Germany.

This research has been sponsored by the EU under SPARK Grant (FP6-2003-IST-004690), by the Banco Santander-Central Hispano-Universidad Complutense de Madrid (Grant PR41/06-15058), by the Spanish Ministerio de Educacion y Ciencia (Grant ESP2004-01511), and by a Ramon y Cajal Grant (awarded to VAM).

Manuscript received xxxxxx, 2007; revised xxxxxx, 2007.

of the gait cycle at which a given limb hits the ground. Then phenomenological models reproducing these features can be introduced and used for robot design. Inspired by this idea the use of oscillatory neural networks with different architectures has been suggested [5], [6].

In fact, most animal gaits possess a degree of symmetry and universal features not far from the behavior of lattice rings of coupled oscillators [7]. For instance coupled nonlinear oscillators can be considered as possible models for locomotor CPGs in insects and other animals [8]-[12]. Then transitions between different gaits can be modeled as switching between different activity patterns in a lattice ring.

Let us now briefly describe the symmetries observable in hexapodal gaits. Fig. 1 illustrates three typical gaits of an insect (for more details see e.g. [9]). We use the following convention: the limbs on the left and right sides are numbered starting from the frontal leg and marked by letters L and R, respectively (Fig. 1A).

When an insect moves slowly, it normally adopts the so called *metachronal* gait (Fig. 1B). This gait can be described as a “wave” propagating forward from the rear of the animal (first on the left side, and then on the right side) according to the scheme:

$$L_3, L_2, L_1, R_3, R_2, R_1.$$

For this gait the adjacent limbs of each half of the insect body (R_3 and R_2 , R_2 and R_1) are 60° out of phase. The limbs of each segment (e.g. R_3 and L_3) are half a period (or 180°) out of phase.

Caterpillar is a medium speed gait at which the motion of the left and right limbs are in synchrony (Fig. 1C) according to the scheme:

$$(L_3R_3), (L_2R_2), (L_1R_1).$$

For relatively fast displacements, the insect adopts the alternating *tripod* gait (Fig. 1D):

$$(L_3L_1R_2), (L_2R_3R_1).$$

In the tripod gait, the ipsilateral anterior and posterior legs, and the contralateral middle leg move together in phase. The limbs of each segment are half a period (180°) out of phase and the adjacent limb on the right and left sides are also half a period (180°) out of phase.

Names like tripod or tetrapod gaits may induce misinterpretation as fixed or rigid gaits. This is not the case as insects (and other animals e.g. crustaceans) play free gait, i.e. the gait characteristics are dynamically changing according to the environment. For example when a small obstacle is on

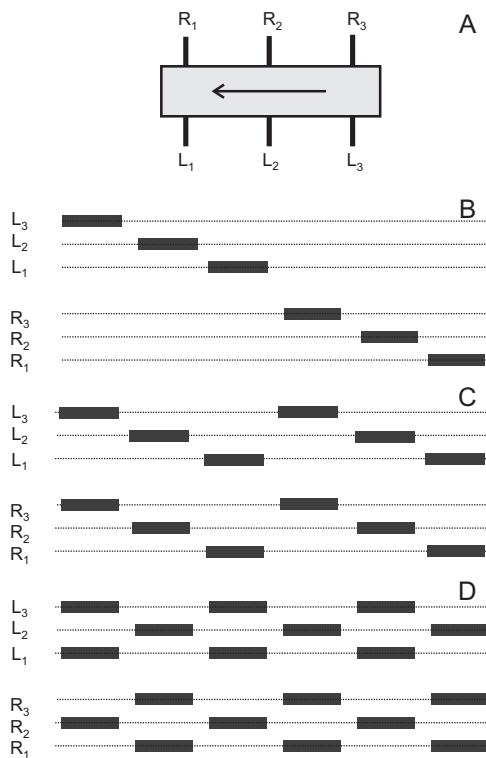


Fig. 1. Sketch of three typical hexapod gaits. A) Leg numbering convention. Letters L and R indicate the left and right sides of the agent, respectively, while the subscript stands for the limb number. B) Metachronal (low – speed) gait. Thick segments show the swing phases (or the return stroke), dotted lines correspond the the stance phases (or the power stroke). Only one leg at a time is lifted and moving forward. C) Caterpillar (medium – speed) gait. D) Tripod (fast – speed) gait.

the path the swing phase of a leg can be shifted or made shorter, thus ensuring smoothness in the animal’s movements. This feature is a real challenge for robot design since a continuous real time adjustment of the CPG cycles is required, which in turn demands fast and sophisticated sensory-motor loops feedbacking information about the environment. The complexity of such an approach has led to shortcomings in most of present-day available walking robots.

In this paper we approach the problem of locomotion control from the nonlinear dynamics viewpoint [13]-[15]. We take advantage of similarities between waves observed in coupled nonlinear oscillators and the symmetries found in animal gaits. In particular, here we consider a lattice ring of coupled oscillators whose nonlinear units or elements have been extensively studied in recent years albeit building upon much earlier work. In our recent works [16]-[18] we have proposed combining a Toda inter-particle nonlinearity [19], [20] with a Rayleigh form of active friction [21] to help maintaining oscillations. We have shown theoretically and numerically the existence and stability of robust propagating waves in such a model problem using a hybrid electro-mechanical analog system. Several hardware implementations of a six-units model have been developed and tested [18]. Here we show that the excitation wave patterns in such a lattice ring of coupled Toda-Rayleigh oscillators have the same symmetries and waveforms as the above mentioned three forward-walking gaits adopted by insects (Fig. 1). In

earlier works [6], [10], [12] gaits have been considered as fixed oscillatory rhythms. However, as earlier noted insects (and other animals e.g. crustaceans) play free gaits, changing rhythms according to the environment. We propose a element composed by a mechanical leg, its actuator (an electrical motor) and an electronic circuit to form a CPG. In this way we incorporate the actuator and leg dynamics in the CPG hence closing the loop CPG – environment – CPG. Thus our approach departs from the concept of fixed gaits and naturally permits to efficiently perform during locomotion over a non-smooth, non-flat environment on a low CPG level with no direct participation of a possible robot upper “brain” or additional, higher level CPG.

II. THE LEG KINEMATICS MODEL

Learning from Nature but not just copying or mimicking it, in this Section we propose a leg kinematics model inspired by the observation of a stick insect (see [22], [23] and references therein). The basic principles upon which we build the model are: i) Minimization of the energy consumption during walking; ii) Autonomous behavior of individual legs also in the presence of small obstacles; and iii) Dynamical coupling of the legs permitting gait adaptability to the environment.

According to biological evidence, a positive feedback in the robot body – coxa (“hip”) and femur – tibia (“knee”) joints has been postulated [24], [25]. This positive feedback involving *elastic* components during walking leads to conservation of gravitational energy [26] observed in insects. At variance with such positive feedback, in our case conservation of the potential energy will not be due to the existence of elastic components in the hexapod robot, but it comes with the mechanical design of the legs.

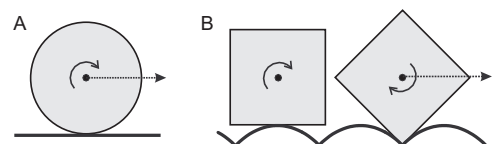


Fig. 2. Examples of displacements preserving potential energy: A) Circular wheel on a flat, horizontal surface; B) Square “wheel” on an inverted catenary.

In order to minimize the energy loss during (linear translatory) motions of the robot with a constant velocity we impose that the robot potential energy is approximately constant. It implies that the vertical position of the center of mass of the robot remains at a given horizontal level. This conservation principle is, for example, satisfied by a wheel rotating over a flat horizontal surface with constant velocity (Fig. 2A). Such motion requires no energy supply. This also can be the case for more complex objects moving over various non-flat surfaces (Fig. 2B). Below we apply this concept to the robot design to drive automatically the robot legs in a way that the initially given potential energy of the robot remains unaltered.

A. The leg stance-swing cycle

Fig. 3 sketches the main elements or modules of an insect leg: coxa, femur, tibia, and tarsus. The modules are coupled

by joints in a way that the leg has nine degrees of freedom though for walking purposes only three are significant as shown by Cruse and collaborators [4], [27]. For the robot design we assume that the leg has only three degrees of freedom controlled by the angles: θ – protraction-retraction of coxa, α – depression-elevation of femur, and β – flexion-extension of tibia. An individual leg can only be in one of two possible functional states: i) stance (or supporting) phase and ii) swing (or recovery) phase.

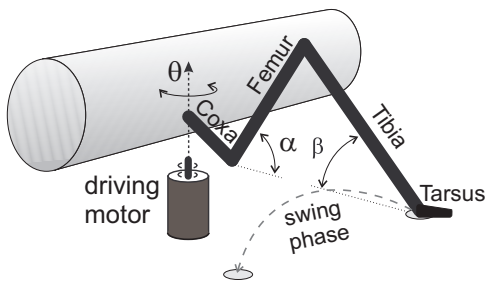


Fig. 3. Schematic diagram showing the main modules of the robot leg inspired by observation of insects. Note the hinge character of the coxa-femur and the femur-tibia joints. A motor inside of the robot body (drawn here outside for easy visualization) drives angle θ controlling protraction-retraction of the coxa according to the leg moving phase. The other angles are functionally coupled to the evolution of θ (see main text).

In the stance phase the tarsus stays on the ground. The movement of the robot can be achieved by the counterclockwise rotation (in Fig. 3) of the angle θ by a driving motor placed inside the robot body. To keep the tarsus fixed on the ground (no sliding) the protraction of coxa (angle θ) is accompanied by an appropriate continuous adjustment of the angles α and β . During the swing (or recovery) phase $d\theta/dt > 0$, the femur angle α increases, the leg is elevated over the ground, moves forward, and then the angle decreases again until the tarsus hits the ground, which generates the swing trajectory of the tarsus (Fig. 3). Thus the evolution of the angle θ functionally determines the behavior of α both in stance and in swing phases. This suggests that if a CPG can control just the angle θ of the legs producing different oscillatory modes (or gaits), then the other angles follow the dynamics of θ_n ($n = 1, 2, \dots, 6$ for six legs). Then an appropriate synchronization of the stance-swing cycles of different legs can be considered in terms of synchronization of angles θ_n only.

B. Leg design: Stance phase

Fig. 4A illustrates schematically our model leg, where for simplicity we use only two segments: femur and tibia, and neglect the lengths of coxa and tarsus. The behavior observed in insects suggests that for walking over a flat horizontal surface, we can approximately assume that both femur and tibia lie in a vertical plane. At rest, i.e. when the robot stays on a horizontal plane, the elevation of the body over the plane is given by the constant H_0 (Fig. 4A) and the leg angles fixed by construction are $\theta = 0$, $\alpha = \alpha_0$, and $\beta = \beta_0$.

At each joint we introduce a circular winding reel (Fig. 4A). One reel is attached to the body during stance phase and

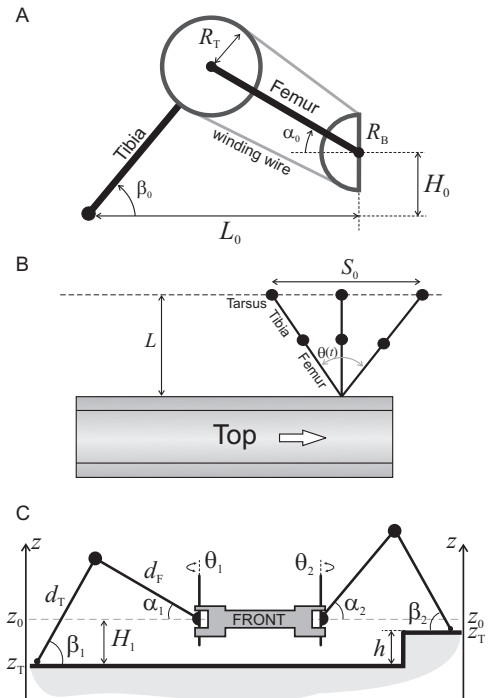


Fig. 4. Mechanical design of the robot. A) The leg configuration at rest. H_0 is the elevation of the robot body (body-femur joint) over the horizontal plane. Angles α_0 and β_0 define initial inclination of femur and tibia, and L_0 is the distance from the body to the tarsus. The leg at each joint has a circular winding reel (not to scale) fixed to the body (during stance phase) and tibia (always). The reels are coupled through a winding wire. When one joint rotates, the wire winds in one reel while unwinding from the other with no sliding. B) The robot top view. Relative successive positions of the L_1 leg for three different values of θ during the stance phase. S_0 is the robot step size. Note that the leg tarsus is fixed on the ground, while the robot body moves forward. C) The robot frontal view. H_n is the vertical distance from the n -th tarsus z_T to the body level z_0 (shown only for the anterior right leg, $n = 1$). All legs in the stance phase adopt a configuration of joints, i.e. values of α and β , such that the body level z_0 remains unaltered.

another to the tibia. According to the angle θ the former rotates always staying in the tibia-femur vertical plane. A wire connecting the two reels can be wound with no sliding on the reels when joints rotate. This mechanical coupling adds a constraint to the angles α and β in the stance phase. We assume the reels to be circular cylindrical with radii R_B and R_T for the body and tibia reels, respectively. Then a change of value in one angle (e.g. Δ_α) leads to the corresponding change of the other angle (e.g. Δ_β):

$$\Delta_\beta = (k - 1)\Delta_\alpha \quad (1)$$

where $k = R_B/R_T$ is the transduction coefficient of the reels. Note that for identical reels the tibia angle β remains constant. Thus the mechanical coupling gives

$$\begin{aligned} \alpha_{\text{stance}}(t) &= \bar{\alpha} + \Delta_\alpha, \\ \beta_{\text{stance}}(t) &= \bar{\beta} + (k - 1)\Delta_\alpha \end{aligned} \quad (2)$$

where $\bar{\alpha}$ and $\bar{\beta}$ are constants to be identified below.

As earlier noted, a leg movement in the stance phase imposes the condition of no tarsus sliding over the ground. Hence the tarsus stays at the same transversal distance L to the body (Fig. 4B) and the femur and tibia angles are coupled

during the coxa protraction (changes of θ) by the constraint

$$d_F \cos \alpha(t) + d_T \cos \beta(t) = L / \cos \theta(t) \quad (3)$$

where d_F and d_T are the lengths of femur and tibia, respectively.

Assuming that the body is the heavier part of the robot (recall that the motors driving the legs are inside the body), we aim at maintaining unaltered the vertical level of the robot center of mass. This implies that during the robot movement with all legs being in stance phase (i.e. on the ground) we should adjust the angles α and β in a way that the vertical coordinate of the coxa of the corresponding leg z_0 remains constant (Fig. 4C).

For a given leg, the distance from its tarsus position z_T to z_0 during the stance phase is given by:

$$H(t) = d_T \sin \beta(t) - d_F \sin \alpha(t). \quad (4)$$

Note that H can vary from leg to leg and depends on the ground profile, i.e. on the presence of obstacles (Fig. 4C, left and right legs). At rest (4) is reduced to $H_0 = d_T \sin \beta_0 - d_F \sin \alpha_0$.

Expanding (4) in a Taylor series and using (2) we obtain

$$H(t) = H^{(0)} + H^{(1)} \Delta_\alpha + O(\Delta_\alpha^2) \quad (5)$$

with

$$\begin{aligned} H^{(0)} &= d_T \sin \bar{\beta} - d_F \sin \bar{\alpha}, \\ H^{(1)} &= (k-1)d_T \cos \bar{\beta} - d_F \cos \bar{\alpha}. \end{aligned} \quad (6)$$

By setting $H^{(1)} = 0$, we have

$$\cos \bar{\beta} = \frac{d_F}{(k-1)d_T} \cos \bar{\alpha}. \quad (7)$$

With (7) satisfied, the variation of H during the stance phase is of second order in Δ_α , which, as we shall see below, gives an error less than 1% for an acceptable range of Δ_α . It is with such ‘‘tolerance’’ or error bar that we can say that energy is maintained ‘‘constant’’.

Given the height of an obstacle h ($h > 0$ for a bump, and $h < 0$ for a trough), we can find the value of $\bar{\alpha}$

$$H^{(0)}(\bar{\alpha}) + h = H_0 \quad (8)$$

where

$$H^{(0)}(\bar{\alpha}) = d_T \sqrt{1 - \left(\frac{d_F}{(k-1)d_T} \cos \bar{\alpha} \right)^2} - d_F \sin \bar{\alpha}. \quad (9)$$

Note that when a leg is on the ground and the robot moves forward, there are no forces from the leg transversal to the body, because the system is in a flat potential region corresponding to a minimum. This means that a small friction between the tarsus and the ground would be enough to prevent sliding of the tarsus perpendicular to the body.

C. Leg design: Swing phase

As earlier mentioned we are seeking a leg design permitting autonomously handling small obstacles solely by the lowest leg (intelligence) level. The robot legs should be able to react to the presence of obstacles on the path in a way that the robot body (i.e. position of the leg coxas) keeps constant its vertical coordinate z_0 (Fig. 4C). This can be achieved only if (7) is satisfied for the stance phases of all legs during all steps.

From (8) follows that the value of $\bar{\alpha}$ depends on the height of the obstacle under the leg tarsus. During walking over uneven ground, at each step the tarsus may be placed at different levels, unknown in advance. Consequently, the value of $\bar{\alpha}$ differs from step to step. On the other hand, (7) must be satisfied and hence the value $\bar{\beta}$ should be adjusted according to (7) at each step. This is only possible if the relationship (7) is satisfied during the whole swing phase, i.e.

$$\cos \beta_{\text{swing}}(t) = \frac{d_F}{(k-1)d_T} \cos \alpha_{\text{swing}}(t). \quad (10)$$

The latter means that the swing phase is not arbitrary, but instead the leg swinging in the air always stays ‘‘prepared’’ for the next stance phase.

A solution is to introduce during the swing phase a mechanical constraint on the leg mechanics to perform a suitable, *ad hoc* swing phase. Fig. 5 shows a possible mechanism

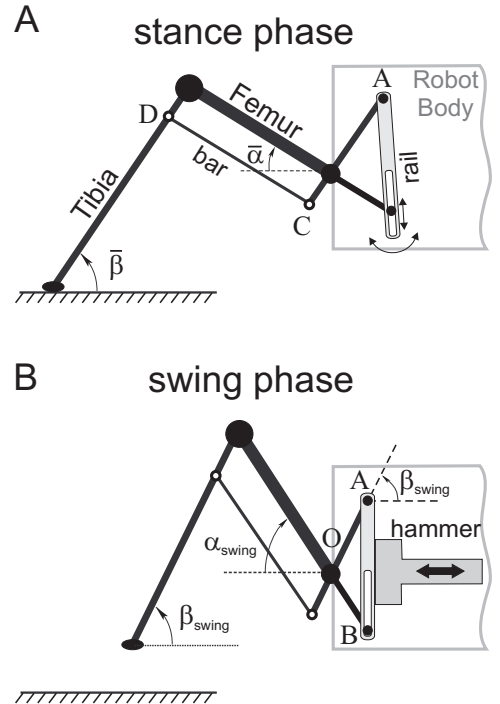


Fig. 5. Leg model design. Implementation of an ‘‘intelligent-like’’ swing phase. A) During stance phase the mechanism produces no constraint on the dynamics of the α and β angles. B) In swing phase the device lifts up the leg.

allowing lifting up the leg over the ground satisfying (10) during the whole swing cycle. It consists of the stabilizing bar DC coupled by freely rotating joints to tibia and the lever CA at points D and C, respectively (Fig. 5A). The bar has the same length as the femur and stays always parallel to it.

During the stance phase, the sliding rail has two degrees of freedom (Fig. 5A) and hence has no effect on the leg dynamics described by (2), (3), and (7). At the beginning of the swing phase, the reel R_B (Fig. 4A) becomes free, so (2) is no more valid. At the same time the rail is maintained in vertical position by the hammer (Fig. 5B), suddenly pushed to the left during the swing phase thus increasing the angle α_{swing} . To complete the swing phase the sliding rail is shifted backwards until the tarsus hits the ground, perhaps, at a different vertical level. Then the reel is attached again to make the next stance phase of the leg movement cycle.

During swing the leg has no degree of freedom, and its motion follows the sliding rail displaced by the hammer. From geometrical considerations (Fig. 5B) we have

$$\overline{OA} \cos \beta_{\text{swing}}(t) = \overline{OB} \cos \alpha_{\text{swing}}(t). \quad (11)$$

Choosing

$$\frac{\overline{OB}}{\overline{OA}} = \frac{d_F}{(k-1)d_T} \quad (12)$$

we satisfy (10) during the swing phase.

With the above described leg design, all H_n remain approximately constant (albeit in general unequal, Fig. 4C) during the robot walk even over a rough ground. This ensures conservation of the vertical coordinate of the robot's center of mass. Hence, energy is only necessary to lift and swing the robot legs that, with our design, demands relatively light energy consumption.

III. SIMULATIONS

In the previous section we have shown that our kinematic model of the leg allows the gait control using only six degrees of freedom (one per leg) given by angles $\theta_1, \dots, \theta_6$. Moreover, it is based on a conservation energy principle thus minimizing energy losses during the robot movement. Let us now illustrate how the model works by performing simulations of walking over different ground profiles. For simulations we use parameter values found for stick insects summarized in Table I [23], [28].

A. The leg dynamics

Using parameter values from Table I we get the leg angles $\alpha_0 = 43^\circ$ and $\beta_0 = 62^\circ$ for $\theta = 0$ that we can take as $\bar{\alpha}$ and $\bar{\beta}$. Note that the parameters $\bar{\alpha}$, $\bar{\beta}$, and L are related through (3), so we have only as free parameter k that can be fixed by using (7). Finally, we have β as a function of Δ_α

$$\beta = \arccos \left(\frac{d_F \cos \bar{\alpha}}{k d_T} \right) + k \Delta_\alpha. \quad (13)$$

Hence, from (3) we have α as a function of θ . This means that according to (9) the body elevation $H(\theta)$ is determined only by θ . Note also that the horizontal position s of the coxa relative to the tarsus, during the stance phase, is given by

$$s(t) = L \tan \theta(t). \quad (14)$$

Thus we have a parametric relation between the body elevation and s as shown in Fig. 6A for a flat surface with $\bar{\alpha} = 30^\circ$. Note

that during motion the leg preserves approximately the robot's potential energy. As earlier mentioned our proposed swing maintains (7). Accordingly, the behavior of the leg during the stance phase does not depend so much on the flatness of the ground, as seen in Figs. 6B and 6C, thus fulfilling item ii) Sect. 2, introduction.

Fig. 6D shows an enlarged view of the body trajectories shown in Figs. 6A, 6B and 6C. Note that the error in the horizontal position of the body increases with increasing step length. In our case, a small increment of potential energy ΔU must be related to a sliding of length ΔL of the tarsus on the ground as

$$F_0 \Delta L = \Delta U \quad (15)$$

where F_0 is the total external force on the tarsus in the direction of its displacement. Note that in the limit of an ideal connecting wire and perfect solid rigid bodies, no elastic energy is stored in the robot and the internal forces do not work. As shown in Fig. 6D, the body elevation remains approximately constant so we have $\Delta U \approx 0$ and then $F_0 \approx 0$. This means that a small friction force of the tarsus $F_{\text{fric}} > F_0$ with the ground will be enough to prevent sliding of the tarsus.

B. Gaits control

Our leg design allows handling small obstacles at the level of each individual leg (Fig. 6). This permits a simple control of the robot movement just by an appropriate driving of the angles $\theta_n(t)$ ($n = 1, 2, \dots, 6$). In order to determine the evolution of the angles we assume that the robot employs one of the gaits shown in Fig. 1. The ratio between the durations of the stance (T_{stance}) and swing (T_{swing}) phases is given by:

$$\frac{T_{\text{stance}}}{T_{\text{swing}}} = \frac{N - m}{m} \quad (16)$$

where N is the number of legs of the robot, and m is the so called mode or gait number. For an hexapod $N = 6$ and we have $m = 1, 2$, and 3 that correspond to the metachronal, caterpillar, and tripod gaits, respectively.

Let us assume that the robot moves with a constant velocity v_0 . Then independently on the gait number duration of the stance phase is

$$T_{\text{stance}} = \frac{S_0}{v_0} \quad (17)$$

where S_0 is the step length. For typical dimensions of a stick insect (Table I) we have $v_0 \approx 4.5$ mm/s and $T_{\text{stance}} \approx 3.3$ s. Using (14) we obtain the dynamics of the protraction-retraction angle in the stance phase (when the tarsus is on the ground):

$$\theta_{\text{stance}}(t) = \arctan \left[\frac{S_0 - 2v_0 t}{2L_0} \right] \quad (18)$$

where $0 \leq t \leq T_{\text{stance}}$. According to (16) and (17) the duration of swing phase depends on the mode number

$$T_{\text{swing}}(m) = \frac{m}{N - m} \frac{S_0}{v_0}. \quad (19)$$

TABLE I
TYPICAL PARAMETER VALUES FOR A STICK INSECT [23], [28].

Body elevation H_0 (mm)	Length of tibia d_T (mm)	Length of femur d_F (mm)	Step size S_0 (mm)	Transversal distance L_0 (mm)	Step frequency (step/min)
7	14	8	15	12	18

The swing phase of the metachronal gait is 2.5 and 5 times shorter than those for caterpillar and tripod gaits, respectively. The angle is then given by

$$\theta_{\text{swing}}(t) = -\arctan\left[\frac{S_0 - 2v_0t(N-m)/m}{2L_0}\right] \quad (20)$$

where $0 \leq t \leq T_{\text{swing}}$. The coordination of the legs is achieved by an appropriate shift of stance-swing cycles (Fig. 1):

$$\theta_n(t) = \theta\left(t + \frac{(n-1)mS_0}{(N-m)v_0}\right). \quad (21)$$

Fig. 7 shows the angle θ_n ($n = 1, 2, \dots, 6$) as a function of time for three different gaits and the corresponding stance-swing cycles very much like the qualitative relationships shown in Fig. 1. Note that usually insects adopt an appropriate gait for walking with a certain velocity, but they also can move with the same velocity employing different gaits. In this case (Fig. 7) the leg dynamics in the stance phase is the same for all gaits [(17), (18)], but the swing phase differs among them being faster for the slower gait [(19), (20)].

IV. ELECTRO-MECHANICAL CPG INTEGRATING THE ACTUATOR AND BODY DYNAMICS IN THE GAIT CONTROL

Fig. 7 shows the evolution of the angles controlling the legs. A minimal CPG should be able to produce the corresponding signal driving the actuator motors. Let us first start with a description of a dynamical systems approach [15] to the generation of rhythms.

A. Toda-Rayleigh lattice ring and its analog circuit implementation

Toda [19], [20] provided exact solutions for a mechanical lattice system (and also for its electric analog system) (Fig. 8A). Six units are coupled by special springs whose force exponentially increases with the decrease of the inter-unit distance (Fig. 8B). Under appropriate limits the exponential Toda interaction reduces to the harmonic oscillator or to the hard sphere interaction.

The Toda system is a conservative one, whereas its circuit implementation unavoidably has energy losses [29]. Thus any excitation of the circuit decays in time and finally vanishes. Accordingly, to maintain oscillations we need to supply energy to the system. One energy-dissipation balance, earlier mentioned, was long ago proposed by Lord Rayleigh [21]. It includes a cubic nonlinearity in the original Toda system regulating the pumping-dissipation balance [17], [18]. Another possibility was proposed by Van der Pol [30].

In view of the above we take a composite conservative-dissipative system. Such a Toda-Rayleigh model [17] in its canonical form is given by:

$$\ddot{x}_n + \omega_0^2(e^{x_n - x_{n+1}} - e^{x_{n-1} - x_n}) - \gamma(\mu - \dot{x}_n^2)\dot{x}_n = 0 \quad (22)$$

where ω_0 is the frequency of linear oscillations, μ is the Rayleigh parameter, and γ accounts for the strength of the Rayleigh cubic nonlinearity in the dynamics of the ring. In the limit $\gamma = 0$ we have the original Toda equation whose exact solution is a cnoidal periodic wave [19], [20].

By allowing γ to be positive or negative we introduce an input-output energy balance hence offering the possibility of maintaining oscillations. In the truly damped case ($\mu < 0$) the system has only one motionless globally stable solution $\{x_{n+1} - x_n = 1\}$. At $\mu = 0$ the system undergoes a symmetric Hopf bifurcation [17], [31], and for $\mu > 0$ the energy balance admits only a discrete set of solutions. $(N-1)$ different oscillatory modes (five for six-units lattice ring) appear in the system [18], [32]. These modes correspond to stable limit cycles coexisting in the $2N$ dimensional phase space of the system. They represent nonlinear waves, similar to waves shown for $\theta_n(t)$ in Fig. 7, propagating along the ring and can be labeled by their wave number m . For the six-units lattice ring (Fig. 8A) the mode $m = 1$ corresponds to a single-peak wave; $m = 2$ to a two-peak waves and $m = 3$ is a mode such that the nearest neighbors move in antiphase (also denoted “optical” mode at variance with the others denoted “acoustic” modes). The sign in the mode number defines the (clockwise or counterclockwise) direction of the wave propagation. Note that since each mode corresponds to a stable limit cycle, only one mode can be realized in the lattice ring at a time with no superposition admitted.

Fig. 9 shows a circuit block-scheme for the Toda-Rayleigh lattice ring consisting of six units (22). Detailed description of all components can be found in [17]. According to the current-voltage (I-V) characteristics of a double capacitor (DC) we have [33]:

$$\frac{d^2V_n}{dt^2} = aI_{dc} \quad (23)$$

where a is a parameter depending on the inner components of the double capacitor. Using Kirchhoff’s laws we get the equations governing the circuit [17], [34]:

$$\frac{d^2V_n}{dt^2} = a(I_n - I_{n+1} + I_{nr}) \quad (24)$$

where I_{nr} is the current through the nonlinear resistor (Fig. 9). I_n represents the current through the junction diode, that can be accurately modeled with

$$I_n = I_s \exp\left(\frac{V_{n-1} - V_n}{V_t}\right) \quad (25)$$

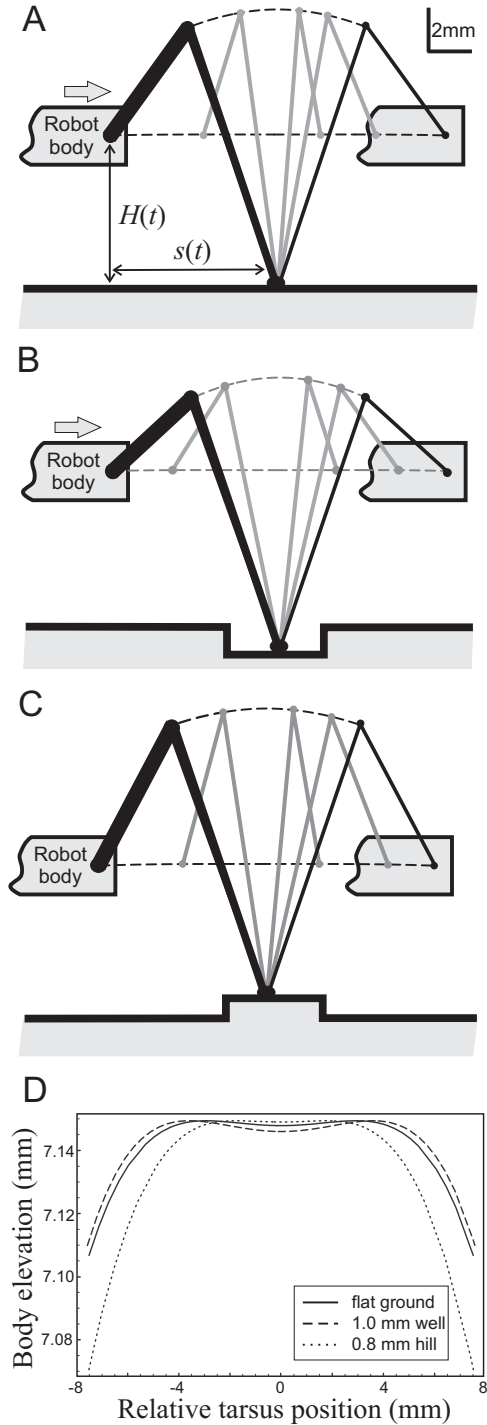


Fig. 6. Leg behavior preserving approximately the potential energy during the stance phase of a step over different ground profiles. Translatory movement of the leg from initial (thick black line) to intermediate (gray) and to final (light black) position over a stance phase. The body moves forward with constant speed. A) A step over a flat ground ($\bar{\alpha} = 45^\circ$); B) A step in a small trough ($\bar{\alpha} = 30^\circ$); C) A step over a small bump ($\bar{\alpha} = 65^\circ$). D) Body elevation $H(t)$ versus tarsus position $s(t)$ during the leg movement in the three cases. The deviation of the body elevation from its initial vertical position does not exceed 1%.

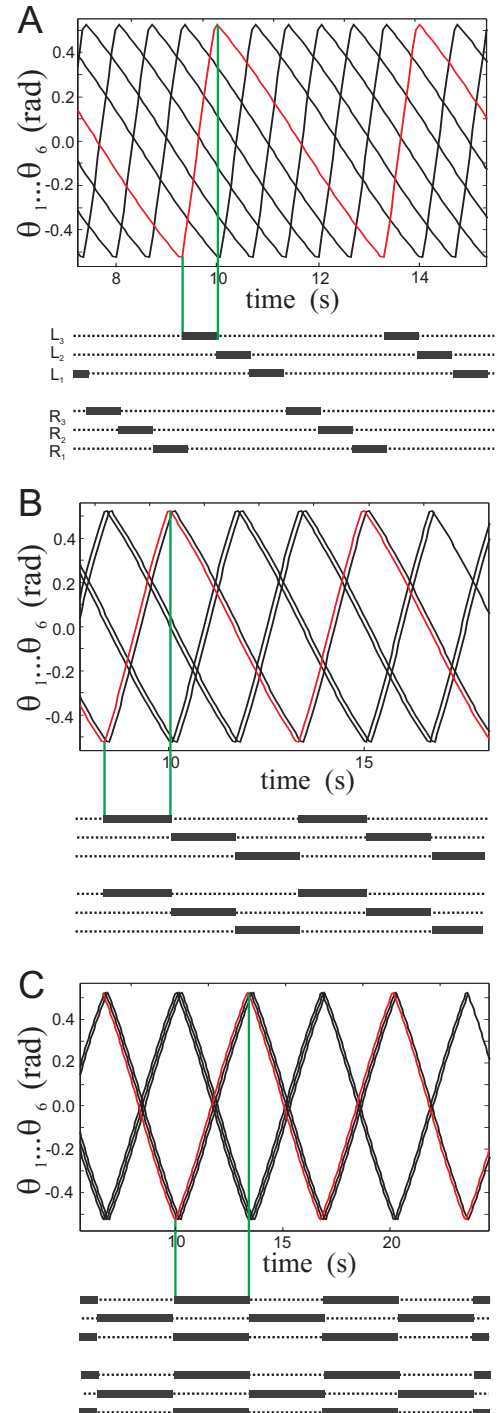


Fig. 7. Hexapod gaits simulations (compare to Fig. 1) and time evolution of the angles controlling the protraction-retraction of the legs during walking for: A) Metachronal, B) Caterpillar, and C) Tripod gaits. Parameter values taken from Table I.

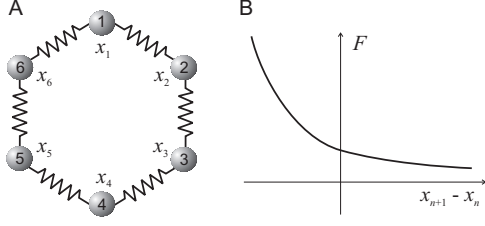


Fig. 8. The Toda ring. A) Six units are coupled in a lattice ring by “exponential springs”. B) Exponential coupling force acting between pairs of neighboring units.

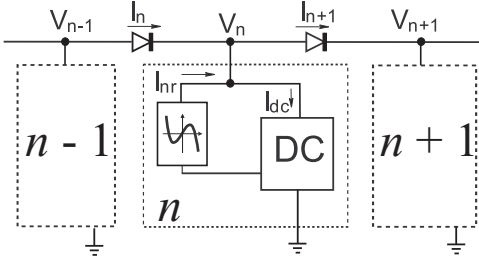


Fig. 9. Block scheme of the Toda-Rayleigh ring. Each unit, n , (encircled by a dashed box) includes two main blocks: a double capacitor (DC) and a nonlinear resistor.

where the constants I_s and V_t depend on the inner diode structure. Thus using diodes we obtain the Toda exponential coupling (Fig. 8B) between neighboring units. The current through the non-linear resistor I_{nr} is a cubic function of the voltage applied to its terminals ΔV that accounts for the Rayleigh energy pumping mechanism

$$I_{nr}(\Delta V) = b \left(\tilde{V}^2 - \Delta V^2 \right) \Delta V \quad (26)$$

where b and \tilde{V} are constants. Finally we have the equation for the voltage V_n of the unit n

$$\frac{d^2 V_n}{dt^2} = a \left\{ I_s \left[e^{\frac{V_{n-1} - V_n}{V_t}} - e^{\frac{V_n - V_{n+1}}{V_t}} \right] + I_{nr} \right\}. \quad (27)$$

Comparing (22) and (26) with (27) one can see that dynamically the circuit described by the voltages V_n is equivalent to the mechanical lattice ring $V_n \propto x_n$.

Fig. 10 shows experimental traces of the three oscillatory modes ($m = 1, 2$, and 3) generated by the Toda-Rayleigh six-units lattice ring. The three modes will lead to the limb movements with symmetries shown in the lower parts of Fig. 10. Comparing the gaits obtained with the Toda-Rayleigh CPG with the actual insect gaits shown in Figs. 1 and 7 we indeed see that the metachronal, caterpillar and tripod gaits are successfully generated by the CPG (Figs. 10A, 10B and 10C).

We can associate each limb with a single oscillator whose dynamics drives through an adaptor the corresponding actuator. The actuator motor rotates according to the voltage dynamics of the corresponding Toda-Rayleigh unit. Thus we can transform the voltage on the unit into angle value,

$$V_n \rightarrow \theta_n. \quad (28)$$

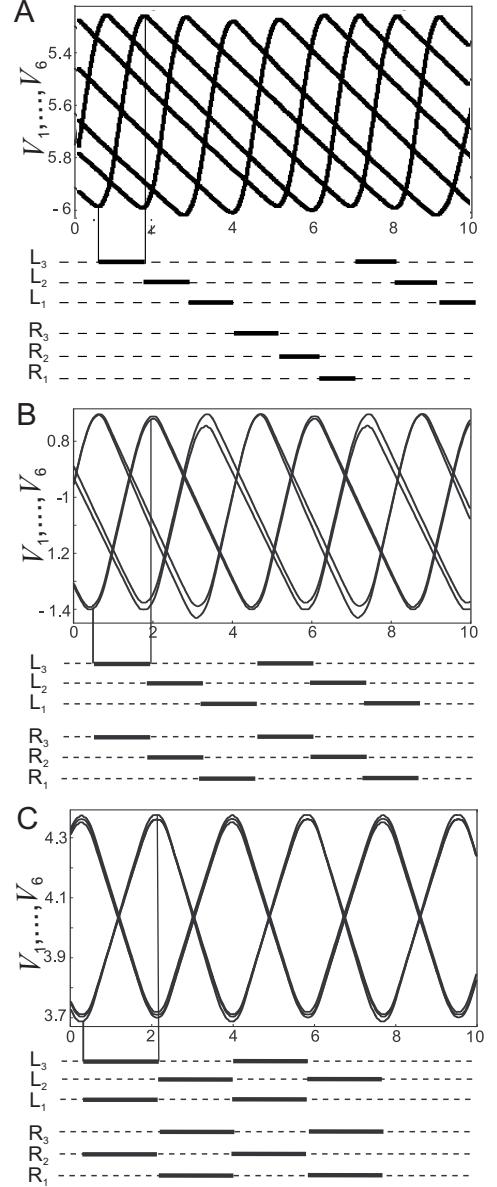


Fig. 10. Oscillatory modes generated by a six-unit Toda-Rayleigh-circuit and their relations to hexapod gaits (compare to Figs. 1 and 7). Upper parts show oscilloscope traces of the voltages from all six units. Bottom parts show the corresponding phase relations. A) The wave mode with $m = 1$ corresponds to the metachronal gait (Fig. 1). B) The mode $m = 2$ corresponds to the caterpillar gait. C) The optical-like mode ($m = 3$) models the tripod gait.

When the voltage derivative is positive we have the swing phase, whereas the negative derivative corresponds to the stance phase. Then the interlimb coordination will naturally follow from the coupling and dynamical interaction of the lattice units. Although having a practical potential such a CPG has a drawback. It produces the same rhythms (fixed gaits) thus having neither account for the dynamics of the robot legs nor for the body.

B. A Central Pattern Generator (CPG) based on the Toda-Rayleigh electro-mechanical circuit

Let us now propose a new circuit implementation for the anharmonic Toda lattice ring that includes the robot current state

as a variable. Thus the new CPG will have a context-dependent dynamics so it will be able to change some characteristics of the gait “on the fly”.

Let us start with the equation of the motor driving a leg. First we note that, in a quite general case, the dynamics of the motor obeys the following equation

$$J \frac{d^2\theta}{dt^2} + f \frac{d\theta}{dt} = I\Phi - T \quad (29)$$

where θ is the angle of the rotor of the motor defining the protraction/retraction of the coxa of the leg, (see Fig. 3), $I\Phi$ is the electromagnetic torque, T is a constant load torque including the internal Coulomb friction, the parameter f is due to the internal viscous friction in the motor that can be taken as a constant, and J is the momentum of inertia. J depends on the inner motor structure and geometrical distribution of the masses. Note that (29) includes the mechanical characteristics of the robot and J is a parameter domain-dependent because it is affected by the global coupling between leg standing on the ground and the body of the robot. Thus we fulfill item iii) Sect. 2, introduction. The current flowing through the motor windings I is given by

$$\ell \frac{dI}{dt} + rI + \Phi \frac{d\theta}{dt} = V_{in}(t) \quad (30)$$

where $V_{in}(t)$ is the input voltage, and Φ is the magnetic flux across the air gap; ℓ and r account for the self (inductance) and the resistance of the motor, respectively.

Usually, each motor leg is driven by an input voltage generated by the CPG (typically a Heaviside step function [35]), while the current through the motor is determined by (30). In our case, the motors are not driven by an input voltage but by the input current I according to (29). In the case of small motors that we use the magnetic flux is generated by a permanent magnet. Then, to a first approximation $\Phi = \Phi_0$ is a constant.

In order to integrate the dynamics of (29) in our Toda-Rayleigh lattice ring we use an angle-voltage converter coupled to the rotor of the motor (Fig. 11)

$$V_n(t) = V_0\theta_n(t) \quad (31)$$

where V_0 is the converter constant. Usually this type of converters are optical devices and do not affect the motor behavior. Then the new variable $V_n(t)$ evolves according to (29):

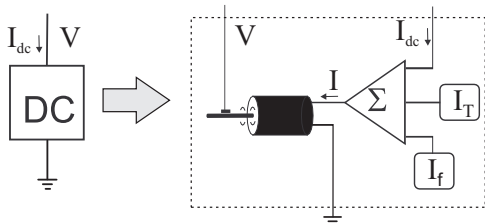


Fig. 11. Block-scheme illustrating how the DC of the CPG (Fig. 9) can be replaced by the electro-mechanical circuit integrating the motor (leg) dynamics.

$$\frac{J}{V_0} \frac{d^2V}{dt^2} + \frac{f}{V_0} \frac{dV}{dt} + T = \Phi_0 I. \quad (32)$$

Now we can split the current $I = I_f + I_T + I_{dc}$ and adjust the values I_f and I_T in such a way that:

$$I_f = \frac{f}{\Phi_0 V_0} \frac{dV}{dt}, \quad I_T = \frac{T}{\Phi_0}. \quad (33)$$

Then from (32) follows:

$$\frac{d^2V}{dt^2} = \frac{V_0}{J} \Phi_0 I_{dc} \quad (34)$$

which is mathematically equivalent to the equation describing the behavior of the double capacitor [(23) and Fig. 11]. Thus we have been able to replace the DC circuit by its electro-mechanical analog. This demands replacing in (27) the factor a by $V_0/J\Phi_0$, which now describes the inner mechanical properties of the leg-motor. We obtain a network where instead of the electronic circuit with double capacitors we use the dynamics of the motors given by (34). Accordingly, the new CPG incorporates a body-leg-motor feedback loop. It produces swing-stance cycles for each leg, similar to those earlier described (Fig. 10), but now directly referring to the angles θ_n (Fig. 7).

Let us finally show how the symmetries of different gaits shown in Fig. 1 can be related to the modes generated by the CPG based on the Toda-Rayleigh electro-mechanical circuit.

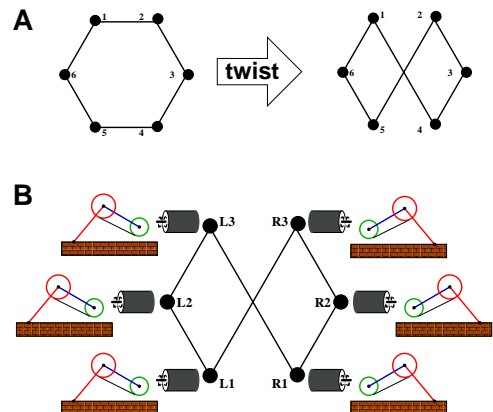


Fig. 12. Electro-mechanical hexapod CPG based on the Toda-Rayleigh six-units lattice ring (see Fig. 8). A) Twisted ring topology. B) Connection scheme of the electro-mechanical Toda-Rayleigh CPG with no intermediate devices between the leg mechanics and electrical circuit.

To accommodate the earlier described oscillatory modes to the gate symmetries we change the initial ring geometry. Fig. 12A illustrates how a new twisted topology can be obtained. For the new topology we have the following sequence of units:

$$2 \rightarrow 3 \rightarrow 4 \rightarrow 1 \rightarrow 6 \rightarrow 5.$$

Note that this sequence is used only for mapping of the units to the limbs, whereas the actual Toda-Rayleigh circuitry remains unchanged. This procedure permits a direct mapping of the wave modes observed in the circuit to the gait symmetries described above. We use the motor-leg as a piece of the CPG with no intermediate device (Fig. 12B). Our CPG generates

not only suitable phase relations between all legs, but also suitable wave forms producing different gaits.

V. CONCLUSION

In this paper we have proposed how to use a nonlinear Toda-Rayleigh lattice ring (Fig. 8) as a central pattern generator (CPG) for controlling hexapodal robots. We have shown that in order to model three different insect gaits, we can use a lattice ring composed of six-units.

First, we have provided a mechanical leg design with three degrees of freedom per leg, two of which are functionally constrained to the leg protraction-retraction angle (Figs. 4 and 5). Then we have shown how a suitable swing phase can be used to prepare the following stance phase in order to keep smooth robot movements even in the presence of small obstacles.

We have shown how a simple leg works maintaining the robot's potential energy practically constant. In this case our CPG is able to control the phases between the legs and also to control the flexion/extension angle between the femur and tibia (see Fig. 6).

To illustrate our results we have built a "circuit" of oscillatory units and have shown that the dynamical behavior of the circuit reproduces the phase relationships found in gaits of a six-legged animal (compare Figs. 1, 7 and 10).

We have also proposed how to incorporate the actuator (motor) dynamics in the CPG (Figs. 11 and 12). With this approach we close the loop CPG – environment – CPG, thus obtaining a decentralized system for the leg control. Our model system does not require further higher level intervention to such CPG for locomotion in a non-flat ground.

Finally, we note that our method based on the nonlinear Toda lattice ring is not limited to the case of six legs. It is possible to implement a $2N$ leg robot by coupling N blocks each with two legs.

ACKNOWLEDGMENT

The authors are grateful to Prof. P. Arena, Prof. J. Ayers, Prof. H. Cruse, Prof. O. Ekeberg, Prof. L. Fortuna, Prof. S. Grillner, Dr. J. Schmitz and Dr. B. Webb for enlightening discussions.

REFERENCES

- [1] E. R. Kandel, J. H. Schwartz and T. M. Jessell, *Principles of Neural Science*. 4th ed. New York: McGraw-Hill, 2000.
- [2] C. A. Wiersma, Ed., *Invertebrate nervous systems*. Chicago: Univ. Chicago Press, 1968.
- [3] H. Cruse, "What mechanisms coordinate leg movement in working arthropods?," *Trends Neurosci.*, vol. 13, pp. 15-21, 1990.
- [4] J. Dean, T. Kindermann, J. Schmitz, M. Schumm and H. Cruse, "Control of walking in the stick insect: from behavior and physiology to modeling," *Autonomous Robots*, vol. 7, pp. 271-288, 1999.
- [5] H. Cruse, T. Kindermann, M. Schumm, J. Dean and J. Schmitz, "Walknet - a biologically inspired network to control six-legged walking," *Neural Net.*, vol. 11, pp. 1435-1447, 1998.
- [6] P. Arena, L. Fortuna and M. Branciforte, "Reaction-diffusion CNN algorithms to generate and control artificial locomotion," *IEEE Trans. Circuits Systems I*, vol. 46, pp. 253-260, 1999.
- [7] W. Y. Yiang, G. Schooner and J. A. S. Kelso, "A synergetic theory of quadrupedal gaits and gait transition," *J. Theor. Biol.*, vol. 142, pp. 359-391, 1990.
- [8] J. J. Collins, and I. Stewart, "Coupled nonlinear oscillators and the symmetries of animal gaits," *Nonlinear Sci.*, vol. 3, pp. 349-392, 1993.
- [9] J. J. Collins and I. Stewart, "Hexapodal gaits and coupled nonlinear oscillator models," *Biol. Cyb.*, vol. 68, pp. 287-298, 1993.
- [10] J. J. Collins and I. Stewart, "A group-theoretic approach to rings of coupled biological oscillators," *Biol. Cyb.*, vol. 71, pp. 95-103, 1994.
- [11] M. Golubitsky, I. Stewart, P. L. Buono and J. J. Collins, "A modular network for legged locomotion," *Physica D*, vol. 115, pp. 56-72, 1998.
- [12] M. Golubitsky, I. Stewart, P. L. Buono and J. J. Collins, "The role of symmetry in animal locomotion," *Nature*, vol. 401, pp. 693-695, 1999.
- [13] L. O. Chua, *CNN: A Paradigm for Complexity*. Singapore: World Scientific, 1998.
- [14] G. Manganaro, P. Arena and L. Fortuna, *Cellular Neural Networks. Chaos, Complexity and VLSI Processing*. Berlin: Springer, 1999.
- [15] V. I. Nekorkin and M. G. Velarde, *Synergetic Phenomena in Active Lattices. Patterns, Waves, Solitons, Chaos*. Berlin: Springer, 2002.
- [16] V. A. Makarov, W. Ebeling and M. G. Velarde, "Soliton-like waves on dissipative Toda lattices," *Int. J. Bifurcation Chaos*, vol. 10, pp. 1075-1089, 2000.
- [17] V. A. Makarov, E. del Rio, W. Ebeling and M. G. Velarde, "Dissipative Toda-Rayleigh lattice and its oscillatory modes," *Physical Rev. E*, vol. 64, pp. 036601-36615, 2001.
- [18] E. del Rio, V. A. Makarov, M. G. Velarde and W. Ebeling, "Mode transitions and wave propagation in a driven-dissipative Toda-Rayleigh ring," *Phys. Rev. E*, vol. 67, pp. 056208-056217, 2003.
- [19] M. Toda, *Theory of Nonlinear Lattices*. Berlin: Springer, 1981.
- [20] M. Toda, *Nonlinear Waves and Solitons*. Dordrecht: Kluwer, 1983.
- [21] J. W. Rayleigh, *The Theory of Sound*. 2nd ed. New York: Dover reprint, 1945, sec. 68a.
- [22] R. D. Quinn, G. M. Nelson, R. J. Bachmann, D. A. Kingsley, J. T. Offi, T. J. Allen and R. E. Ritzmann, "Parallel complementary strategies for implementing biological principles into mobile robots," *Int. J. Robotics Res.*, vol. 22, pp. 164-186, 2003.
- [23] M. Schumm and H. Cruse, "Control of swing movement: influences of differently shaped substrate," *J. Comparative Physiol. A*, to be published.
- [24] H. Cruse, C. Bartling and T. Kindermann, "High-pass filtered positive feedback for decentralized control of cooperation," in *Advances in Artificial Life*, F. Moran, A. Moreno, J. Merelo and P. Chacon, Eds. New York: Springer-Verlag, 1995, pp. 668-678.
- [25] T. Kindermann, "Behavior and adaptability of a six-legged walking system with highly distributed control," *Adapt. Behav.*, vol. 9, pp. 16-41, 2002.
- [26] A. Schneider, H. Cruse and J. Schmitz, "A Biologically Inspired Active Compliant Joint Using Local Positive Velocity Feedback (LPVF)," *IEEE Trans. Systems, Man, and Cyb. - Part B: Cyb.*, vol. 35, pp. 1120-1130, 2005.
- [27] J. Schmitz, J. Dean, T. Kindermann, M. Schumm and H. Cruse, "A biologically inspired controller for hexapod walking: simple solutions by exploiting physical properties," *Biol. Bull.*, vol. 200, pp. 195-200, 2001.
- [28] V. Dürr, J. Schmitz and H. Cruse, "Behaviour-based modelling of hexapod locomotion: linking biology and technical application," *Arthropod Struct. & Devel.*, vol. 33, pp. 237-250, 2004.
- [29] A. C. Singer and A. V. Oppenheim, "Circuit implementations of soliton systems," *Int. J. Bifurcation Chaos*, vol. 9, pp. 571-590, 1999.
- [30] B. Van der Pol, "On 'relaxation-oscillations'," *Phil. Mag.*, vol. 2, pp. 978-992, 1926; "Forced oscillations in a circuit with non-linear resistance," *Phil. Mag.*, vol. 3, pp. 65-80, 1927.
- [31] Yu. A. Kuznetsov, *Elements of Applied Bifurcation Theory*. Berlin: Springer-Verlag, 1995.
- [32] V. A. Makarov, M. G. Velarde, A. Chetverikov and W. Ebeling, "Anharmonicity and its significance to non-Ohmic electric conduction," *Phys. Rev. E*, vol. 73, pp. 066626-066612, 2006.
- [33] P. Horowitz and W. Hill, *The Art of Electronics*. Cambridge: Cambridge University Press, 1987.
- [34] N. Islam, J. P. Singh and K. Steiglitz, "Soliton phase shifts in a dissipative lattice," *J. Appl. Phys.*, vol. 62, pp. 689-693, 1987.
- [35] S. Still, K. Hepp and R. J. Douglas, "Neuromorphic walking gait control," *IEEE Trans. Neural Netw.*, vol. 17, pp. 496-508, 2006.



Ezequiel del Rio graduated in Physics at the Universidad Complutense de Madrid (Spain) in 1987, and received the Ph.D. degree in Physics from the same University in 1992. He currently is an Associated Professor with Applied Physics Department, Universidad Politecnica de Madrid (Spain). His research interests include nonlinear lattice dynamics and its applications.



Valeri A. Makarov graduated in Physics at the Nizhny Novgorod State University (Russia) in 1992, and received the Ph.D. degree in Physics and Mathematics from the same University in 1997. From 1998 he is with the Universidad Complutense de Madrid (Spain). His research interests are in nonlinear dynamics, time-series analysis and their applications in neuroscience.



Manuel G. Velarde graduated in Physics at the Universidad Complutense de Madrid (Spain) in 1963, and received the Ph.D. degree in Physics from the same University in 1968 and from the Universite Libre de Bruxelles (Belgium) in 1970. He currently is Professor of Physics and Head of Department at Instituto Pluridisciplinar of Universidad Complutense. His research interests cover a wide domain from fluid physics to nonlinear dynamics at large (<http://www.ucm.es/info/fluidos>). Presently, he is research concentrates on nonlinear lattice dynamics

and its applications.



Manuel G. Bedia is a B. S. in Physics (1995), M. Sc. in Physics (Applied physics, 1997), M. Sc. Technological innovation management (1999) and Ph. D. in Computer Science (2004). He has been Technological Consultant in Technology innovation, knowledge management and development in information technology. Currently, he is Associate Professor of Computer Science (University Charles III, Madrid) and he collaborates as researcher at the Pluridisciplinar Institute (University Complutense, Madrid) developing models inspired by the basic

principles of living systems and based on the idea of self-organization. He has worked on several Artificial Intelligence (AI) Research projects sponsored by Spanish and European Institutions.